Journal of Catalysis 300 (2013) 102–112

Contents lists available at SciVerse ScienceDirect

Journal of Catalysis

journal homepage: www.elsevier.com/locate/jcat

A comparative study of glycerol dehydration catalyzed by micro/mesoporous MFI zeolites

Luiz Gustavo Possato [a], Rosiane N. Diniz [a], Teresita Garetto [b], Sandra H. Pulcinelli [a], Celso V. Santilli [a], Leandro Martins [a,*]

[a] Instituto de Química, UNESP – Univ Estadual Paulista, Prof. Francisco Degni 55, 14800-900 Araraquara, SP, Brazil
[b] INCAPE – Instituto de Investigaciones en Catálisis y Petroquímica, Santiago del Estero 2654, Santa Fe, Argentina

ARTICLE INFO

Article history:
Received 28 November 2012
Revised 7 January 2013
Accepted 7 January 2013

Keywords:
Mesoporous materials
Zeolites
Glycerol dehydration
Acrolein
Deactivation

ABSTRACT

The catalytic properties of monomodal microporous and bimodal micro-mesoporous zeolites were investigated in the gas-phase dehydration of glycerol. The desilication methodology used to produce the mesoporous zeolites minimized diffusion limitations and increased glycerol conversion in the catalytic reaction due to the hierarchical system of secondary pores created in the zeolite crystals. The chemical and structural properties of the catalyst were studied by X-ray diffraction, nitrogen adsorption–desorption isotherms, NH_3-TPD and pyridine chemisorption followed by IR-spectroscopy. Although the aim was to desilicate to create mesoporosity in the zeolite crystals, the desilication promoted the formation of extra-framework aluminum species that affected the conversion of glycerol and the products distribution. The results clearly show that the mesoporous zeolites with designed mesopore structure allowed a rapid diffusion and consequently improved the reaction kinetics. However, especial attention must be given to the desilication procedure because the severity of the treatment negatively interfered on the Brønsted and Lewis acid sites relative concentration and, consequently, in the efficiency of the catalysis performed by these materials. On the other hand, during the catalytic reaction, the intracrystalline mesopores allowed carbonaceous compounds to be deposited herein, resulting in less blocked micropores and catalysts with higher long-term stability.

© 2013 Elsevier Inc. All rights reserved.

1. Introduction

The increase in production of glycerol through transesterification of fats or vegetable oil provides chances of studying new technological applications for uses of glycerol as raw material. The value of glycerol contributes to the cost competitiveness of biodiesel processes because about 1 kg of glycerol is formed for each 9 kg of biodiesel produced. As a consequence, the transformation of glycerol into more valuable products is desirable and essential since it improves the economics of the biodiesel production and, at the same time, may provide the industry with important and versatile feedstocks [1]. Etherification, oxidation, reforming, and esterification are examples of reactions in which glycerol may be consumed [2]. The transformation of glycerol into synthesis gas and subsequently the Fisher–Tropsch reaction for the production of hydrocarbons is an additional application [3]. Dehydration is one of the interesting uses of glycerol, and acrolein is the major product.

Commercial production of acrolein by the catalytic condensation of formaldehyde and acetaldehyde was firstly established in 1942 by Degussa, and nowadays, the main route is the oxidation of propylene catalyzed by mixed bismuth and molybdenum oxides [4]. Therefore, there is the possibility of the synthesis of acrolein by a renewable route with the use of glycerol minimizing the use of petrochemical resources as raw material. The acrolein is an intermediate used for the production of acrylic acid esters, adhesive, superabsorber, polymers, and detergents [5]. An important technological advance would be the development of a process for the production of acrylic acid in one step from glycerol. An alternative study is double-bed with two catalysts [6] or, which is more interesting, the development of bifunctional catalysts that can selectively dehydrate glycerol and subsequently oxidize acrolein to acrylic acid.

Various catalysts have been studied in the heterogeneous catalysis for dehydration of glycerol, such as $MeO–Al_2O_3–PO_4$ (Me: transition metal) [7], WO_3/TiO_2 [8], other types of mixed oxide catalysts such as molybdenum/tungsten [5] and zeolites as MFI, BEA, FAU, and MOR with different Si/Al ratios [9]. The main similarities between these catalysts are the presence of acid sites responsible for the dehydration of glycerol. Dehydration of the central hydroxyl leads to 3-hydroxy-propanal, which can also undergo dehydration to form acrolein. On the other hand, a parallel reaction can occur: the dehydration of terminal hydroxyl groups

* Corresponding author. Fax: +55 16 3322 2308.
E-mail address: leandro@iq.unesp.br (L. Martins).

0021-9517/$ - see front matter © 2013 Elsevier Inc. All rights reserved.
http://dx.doi.org/10.1016/j.jcat.2013.01.003

that leads to acetol [10]. The formation of acrolein is related to the Brønsted acid sites, while the Lewis acid sites generally show higher selectivity for acetol [1].

The application of zeolites as highly active, selective, and stable catalysts in large-scale technologies is widespread [11–13]. However, the catalytic conversion of glycerol is hindered in microporous systems restricted by the transport of molecules in the channels of the zeolitic structure and also obstruction of the pores by the deposition of coke during the reaction. The methodology for minimizing diffusion limitations and increasing efficiency involves the production of hierarchically structured zeolites, characterized by the formation of secondary pores in the mesopore region (2–50 nm) in the zeolite crystals [14]. For example, Chal et al. discussed strategies for the synthesis of zeolites with micro- and mesopores including destructive synthesis (dealumination and desilication) or by constructive synthesis strategies (zeolitization of mesoporous materials). In a particular case, the extraction of silicon from the zeolite framework in alkaline medium has proved to be a simple treatment to provide mesoporosity in zeolites [15].

The selective dehydration of glycerol to acrolein can be achieved using a great variety of acid catalysts and experimental conditions. However, in the case of solid catalysts, additional to the acidity, the textural properties also play an important role in this process. The gas-phase reaction is usually better than the liquid-phase reaction for the dehydration of glycerol because the glycerol conversion and acrolein selectivity can be easily modified with parameters such as flow of glycerol, temperature reaction, and mass of catalyst [6].

In this study, we compare and discuss the catalytic dehydration in the gas phase of glycerol to acrolein using microporous MFI zeolites and desilicated ones. In the study, the effect of desilication in the conversion of glycerol, the distribution of the products, and also the control of diffusion constraints and deactivation by different location of coke formation in the pores is shown.

2. Experimental

2.1. Catalysts

The various MFI zeolites kindly provided by Zeolyst (USA) were initially used in the sodium form. Throughout the manuscript, the following nomenclature has been adopted for the parent (1) MFI15, MFI25, and MFI40 zeolites, where the number is related to the Si/Al molar ratio and (2) for the desilicated MFI40 zeolite: MFIOH*x*, where *x* stands for the NaOH to silicon in zeolite molar ratio ($x = OH^-/Si$). Different alkaline treatments of the MFI40 zeolite were performed in an aqueous 0.2 mol/L NaOH solution at a temperature of 40 °C. To do that, 1 g of this zeolite was put in a polypropylene flask and vigorously stirred for 1 h in a specific volume of alkaline solution, which was adjusted to give hydroxyl to silicon molar ratio of 0.2, 0.4, 0.6, 0.8, and 1.2. The resulting suspension was cooled in water, centrifuged, and then washed with 200 mL distilled water three times. The dried products were converted in the H-form by three consecutive exchanges in 0.1 mol/L NH_4NO_3 solution and subsequent calcination at 500 °C (heating rate = 5 °C/min) for 2 h under air atmosphere.

2.2. Catalyst characterization

The crystalline phases present in calcined samples were analyzed by X-ray diffraction using a Siemens D5000 diffractometer and Cu Kα radiation selected by a curved graphite monochromator. Data were collected in the 2-theta range from 5° to 40° using a step size of 0.01° and counting time of 4 s. For the unit cell parameters determination, the database of powder diffraction file of International Zeolite Association was used. The refinement procedure was started using the known unit cell dimension of the ammonium form and the monoclinic crystal system ($a \neq b \neq c$ and γ). Cell dimensions of zeolite samples were calculated from 10 measured peaks on the average. The different angles between T–O–T bonds (where T represents silicon or aluminum atoms tetrahedrally coordinate in the zeolite framework) allow each zeolite structure to contract and expand at a different level upon response to variables like temperature, framework composition, as well as upon guest molecules present in the pores.

Nitrogen adsorption–desorption isotherms were recorded at liquid-nitrogen temperature and relative pressure interval between 0.001 and 0.998 on a Micromeritics (ASAP 2010) equipment, which was used to assess the created mesoporosity. Samples were evacuated prior to measurements at 200 °C for 12 h under vacuum of 1×10^{-5} Pa. The *t*-plot was applied to determine the individual contributions from micro- and mesoporosity, and the mesopore size distribution was estimated by the BJH pore size model. The mesopore volume was determined according to: $V_{meso} = V_p - V_{micro}$, where V_p and V_{micro} are the total volume of pores and the volume of micropores, respectively.

The zeolite crystals size and morphology were observed by scanning electron micrographs on a Philips XL30 microscope. The samples were previously deposited on aluminum sample holder and sputtered with gold.

The solid-state ^{27}Al NMR spectra were recorded using a Varian INOVA 500 spectrometer equipped with a 7 mm probe at spinning rate of 4.5 kHz. The ^{27}Al chemical shifts were referenced to a 1.0 mol/L $Al(NO_3)_3$ aqueous solution. The experimental conditions were operating frequency of 78.2 MHz, acquisition time of 15.4 ms, pulse-width of 2.4 μs, and recycle delay of 0.1 s. For each spectrum, 256 scans were acquired.

The acid property of the catalysts was characterized by ammonia temperature programmed desorption (NH_3-TPD). In all the experiments, 150 mg of sample was outgassed at 300 °C for 1 h in flowing helium (60 mL/min) and then cooled down to 100 °C. At that temperature, the sample was exposed to a flow of 60 mL/min of 1% of ammonia in helium, for 1 h. After the adsorption of ammonia reached saturation, the sample was flushed at 100 °C for 1 h with helium to remove excess ammonia, and then, the temperature was programmed at 10 °C/min up to 700 °C in flowing helium at 60 mL/min. The amount of desorbed ammonia per gram of sample was monitored and estimated by the mass spectrometer response.

The thermogravimetric analysis of the used catalysts after the reaction was carried out under air (100 mL/min) using a TA SDT Q600 TGA/DSC thermobalance in the range of 30–900 °C at heating rate of 10 °C/min.

Infrared spectroscopy (FTIR) was recorded by using a Shimadzu Prestige IR apparatus. The catalysts samples (*ca.* 50 mg) were pressed as thin disks (2 ton/cm^2), with a diameter of approximately 25 mm. Before pyridine adsorption, all samples were pretreated in an all-glass high-vacuum system at 300 °C for 30 min under pressure of 0.013 Pa. For the adsorption experiments, the samples were cooled down to 150 °C under vacuum and then 2 μL of liquid pyridine was injected. Spectra were recorded after evacuation for 60 min at 200 °C. The background spectrum, recorded under identical operating conditions without sample, was always automatically subtracted. The relative concentration of the Brønsted and Lewis acid sites was calculated from the intensity of the PyH^+ and PyL bands (1545 and around 1450 cm^{-1}, respectively).

2.3. Catalytic reactions – glycerol and ethanol dehydration

The catalytic dehydration reaction was carried out in the gas phase at 300 °C [8,16] under atmospheric pressure in a continuous

flow glass fixed-bed reactor inside a hot box at 180 °C to avoid condensation of products. Prior to the catalytic tests, 100 mg of the acid zeolite was heated up to 300 °C under nitrogen flow (15 mL/min) and kept at this temperature for 15 min to remove adsorbed water. After that, the bypass valve was turned off allowing the mixture of glycerol and carrier gas to flow through the reactor (time zero). The bypass valve was started after the whole system (tubes and valves) had been previously saturated and operated in steady state. Glycerol was used as received (99 wt.%, Sigma–Aldrich). The composition of fed glycerol solution was 10 wt.% in water, the flow of this solution was 0.1 mL/min controlled by HPLC pump (GILSON 307), and N_2 was used as carrier gas (15 mL/min). The solution and the gas were fed to the reactor through a heated line at 180 °C. The use of nitrogen as a carrier gas was to guarantee that the reactants and products formed at the very last minutes of reaction were transported more efficiently and collected in the gas–liquid separator kept at 4 °C. Because glycerol is a high-boiling liquid, it will not behave as the water component of the solution would; therefore, the use of nitrogen helps in a more efficient transport of glycerol through catalytic reactor. In order to confirm that the precautions we had taken were suitable for the glycerol dehydration experiments, we collected samples using an empty reactor, that is, without catalyst, and we could verify steady-state flow and composition after starting the bypass valve. The products collected in the gas–liquid separator were analyzed by gas chromatography (Shimadzu GC-2014) equipped with a capillary column (Rtx-1, 30 m, 0.32 mm, 1 μm) and FID detector. Before each injection, a known mass of *n*-butanol was added as internal standard. The analyses were done in triplicate. The retention times were compared with those of authentic compounds. Conversion of glycerol ($X_{glycerol}$) and products selectivity (S) were calculated according to equations:

$$X_{glycerol}\ (\%) = \frac{n_{Gl}^{input} - n_{Gl}^{output}}{n_{Gl}^{input}} \times 100 \quad (1)$$

$$S\ (\%) = \frac{n_i}{n_{Gl}^{input} - n_{Gl}^{output}} \times \frac{Z_i}{Z_{Gl}} \times 100 \quad (2)$$

where n_{Gl}^{input} and n_{Gl}^{output} are the molar flow of glycerol in the input and output (mol/min); n_i the molar flow of products i (mol/min); $Z_{Gl} = 3$ and Z_i represent the number of carbon atoms in the molecule of glycerol and in the products, respectively [7].

The glycerol conversion at time zero was estimated based on the extrapolation of a fitted exponential decay according to:

$$X_{glycerol}^{0}(\%) = A \cdot \exp(-t/B) \quad (3)$$

The relative deactivation (D) of the catalysts used in the glycerol dehydration was calculated according to:

$$D\ (\%) = \frac{(X_{glycerol})_{at\ time\ zero} - (X_{glycerol})_{after\ 8h}}{(X_{glycerol})_{at\ time\ zero}} \times 100 \quad (4)$$

In order to compare the different catalysts in a non-deactivating reaction and to eliminate the influence of coke deposits on the interpretation of diffusional characteristics of the samples, the ethanol dehydration reaction was used as a model reaction. The catalytic dehydration of ethanol was carried out in the gas phase at 230 °C using the same procedure of glycerol dehydration, apart from that ethanol was fed as received (99 wt.%, Qhemis) at a flowing rate of 0.1 mL/min.

3. Results and discussion

3.1. Catalysts modification and characterization

The results of elemental composition and the nitrogen adsorption/desorption on parent and modified MFI zeolites are presented in Table 1. The textural properties confirm that the majority of the zeolites contain micropores and the contribution of mesopores is varied according to the desilication procedure. Microporosity prevails in all the isotherms, as can be derived from the high nitrogen uptake at very low pressures. Upon alkaline treatment, the isotherm of MFI samples (Fig. 1) experiences alteration of the adsorption properties, due to framework silicon extraction and mesopore formation [17]. The volume of mesopores (V_{meso}) increases but of the micropores (V_{micro}) decreases, which depends on the degree of their microstructural collapse. The micropore sizes are related to the MFI zeolite structure, that is, composed of 0.55-nm-wide sinusoidal channels along the *a*-axis and of 0.53-nm-wide straight channels along the b-axis. The mesopore sizes created after the desilication concentrate on the range of 10–40 nm (Fig. 1B), presenting broad distribution and irregular morphologies. The slight mesopore volume detected in MFI40 sample is mainly a result of the aggregated nature of small crystals that leads to a relatively intercrystalline porosity.

Powder X-ray diffraction patterns (Fig. 2) have confirmed that the characteristic of the zeolite structure is maintained, although the intensity of most of the well-resolved reflections has decreased for MFIOH12 sample, promoting some loss of crystallinity due to the severity of the treatment.

The scanning electron micrographs of samples MFI40, MFIOH04, MFIOH08, and MFIOH12 (Fig. 3) upon alkaline treatment reveal the overall size and morphology of the outer surface of the zeolite crystals are significantly affected. This corroborates with the pore size distribution, indicating the increase in volume of nitrogen adsorbed by the zeolite with the progress of the degree of desilication. Initially, the parent sample MFI40 consists of aggregated nanometer-sized crystals in the micrometer range, and for

Table 1
Chemical composition and textural properties of the parent and desilicated MFI40 zeolites in the H^+-form. A commercial alumina sample was included as a reference.

Treatment	Samples	Si/Al_{Global}[a]	$Si/Al_{Framework}$[b]	f_{Al}[c]	V_{micro} (mL/g)	V_{meso}[e] (mL/g)
Parent zeolites	MFI15	15	...	0.063	0.26	0.0
	MFI25	25	...	0.038	0.28 (0.00)[d]	0.0 (0.00)
	MFI40	40	39.5	0.024	0.25	0.0
Desilicated MFI40	MFIOH02	34	39	0.029	0.24	0.32
	MFIOH04	29	33	0.033	0.22	0.48
	MFIOH06	18	31	0.053	0.17 (0.00)	0.76 (0.77)
	MFIOH08	11	26	0.083	0.13	1.40
	MFIOH12	08	29	0.111	0.08	2.07
Reference	Al_2O_3	...	...	1.000	0	0.89

[a] Global silicon to aluminum molar ratio.
[b] Framework silicon to aluminum ratio estimated from deconvolution of ^{27}Al NMR spectra.
[c] Molar fraction of aluminum (Al/(Si + Al)) calculated on the basis of global silicon to aluminum molar ratio.
[d] In brackets are indicated the micro- and mesoporous volume of the spent catalysts, measured after 8 h of use in the dehydration of glycerol.
[e] The volume of mesopores (V_{meso}) where calculated according to $V_{meso} = V_p - V_{micro}$.

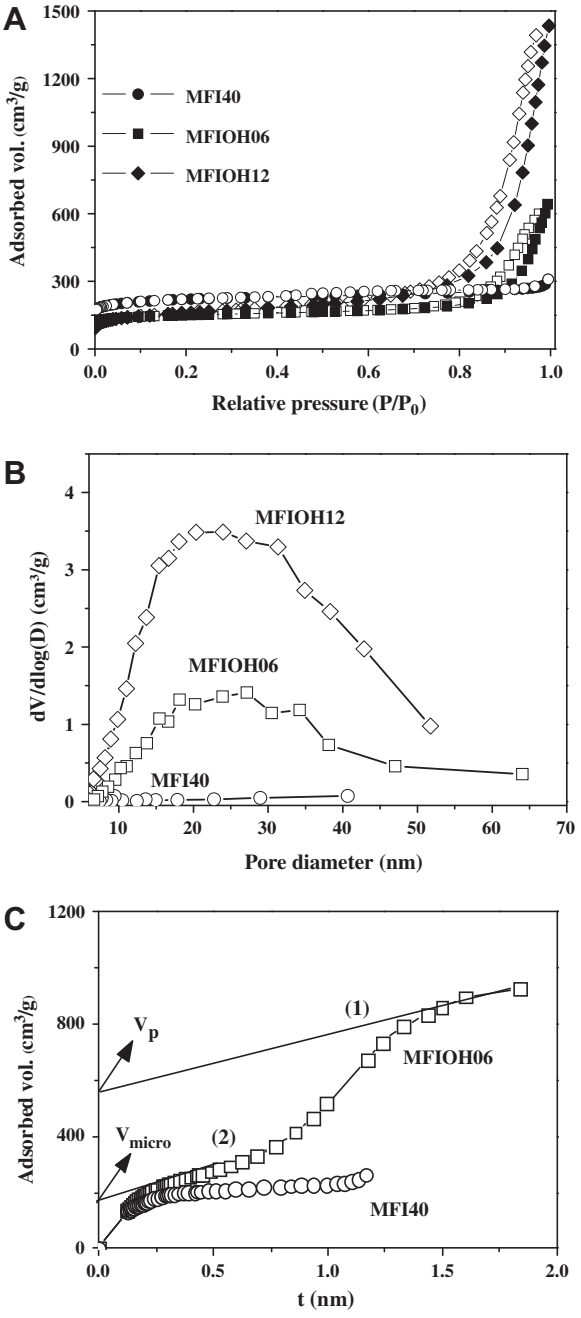

Fig. 1. (A) Nitrogen adsorption–desorption isotherms (filled points correspond to nitrogen adsorption and empty points to desorption), (B) BJH pore size distribution based on desorption branch of the isotherms of parent MFI40 and desilicated MFIOH06 and MFIOH12 zeolites, (C) *t*-plot graphic showing the regions used to determine the micro (straight line 1) and mesoporous volume (straight line 2).

the treated samples, particle deagglomeration occurs due to dissolution of silicon in the boundaries of the crystal. This can be evidenced by the observation of MFIOH12 crystals, which are rough and form a sponge-like morphology, completely distinguishable from the original zeolite.

For further investigation of the desilication process, samples were examined by solid-state ^{27}Al MAS NMR because the aluminum is also removed from the zeolite structure in an unavoidable manner during the desilication. According to the spectra, tetrahedrally coordinated framework aluminum in hydrated zeolites consist of a single signal in the chemical shift around 54 ppm (identified as AlO_4 in Fig. 4), which is evident in the parent sample

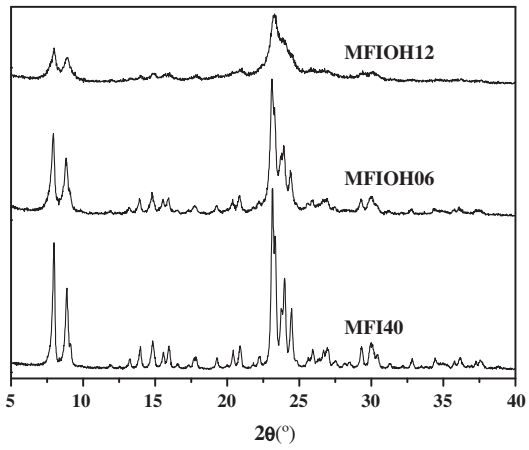

Fig. 2. X-ray powder diffraction patterns of the parent MFI40 and desilicated MFIOH06 and MFIOH12 zeolites.

MFI40. However, for desilicated MFI40 samples, this peak is lower and broadens (Table 2) because of the contribution of non-framework aluminum species that appears in the range of 30 to −13 ppm and to tetrahedrally distorted Al species, respectively [9]. Although the purpose was to remove silicon, aluminum might also be removed depending on the severity of the desilication process. For example, very broad and overlapped resonance peaks observed for MFIOH12 sample (Fig. 4B) is a spectral characteristic associated with non-framework Al species with different oligomeric sizes, neutral or ionic that counts negatively to the acid character of the zeolites, reducing the amount and the acid strength of acid sites.

The relative intensity of the peaks corresponding to the aluminum species (Table 2) allowed to the approximate calculation of the framework silicon to aluminum ratio (Si/Al_F) presented in Table 1. Fig. 4B shows the deconvoluted peaks which were integrated for sample MFIOH12. The peaks related to the family of hexacoordinated aluminum species (AlO_6) are assigned to indefinite polymeric oxyhydroxy aluminum aggregates or to ionic particles that might act as charge balancing cation in the zeolite structure. Despite the complex composition of non-framework aluminum this scenario seems probable, because as the severity of desilication and the amount of alkaline solution increase, the contribution of hexacoordinated aluminum is also higher. The families of non-framework aluminum species influence negatively the catalysis performed by zeolites if pores are blocked and accessibility to active sites hindered [18,19]. Furthermore, ionic species might also exchange protons (Brønsted acidity) and compensate for the framework charge resulting in less dense acid sites. To prove that we treated sample MFIOH06 in 0.5 mol/L oxalic acid solution for 1 h under reflux, and the contribution of isolated hexacoordinated aluminum species diminished from 23.5% to 15.2% probably due to leaching of ionic species [20].

3.2. Surface acidity

In addition to the pore structure, the amount and strength of acid sites are also decisive factors determining the catalytic functions of the zeolites. In this respect, we analyzed the acidity of the materials by temperature programmed desorption of ammonia (NH_3-TPD) and pyridine chemisorption by infrared spectroscopy (Py-FT-IR) followed by desorption of weakly bounded species, before and after the alkaline treatment. Considering that the TPD method could mislead the interpretation of acidic properties, such as readsorption of ammonia, overlapping of peaks and strong

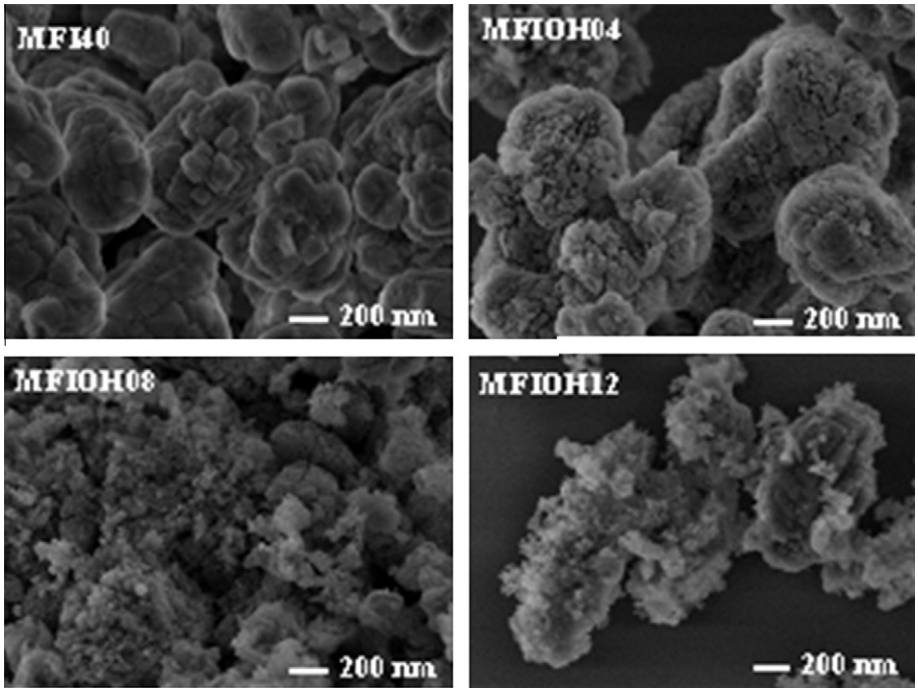

Fig. 3. Scanning electron micrographs of parent MFI40 and desilicated MFIOH04, MFIOH08, and MFIOH12 zeolites.

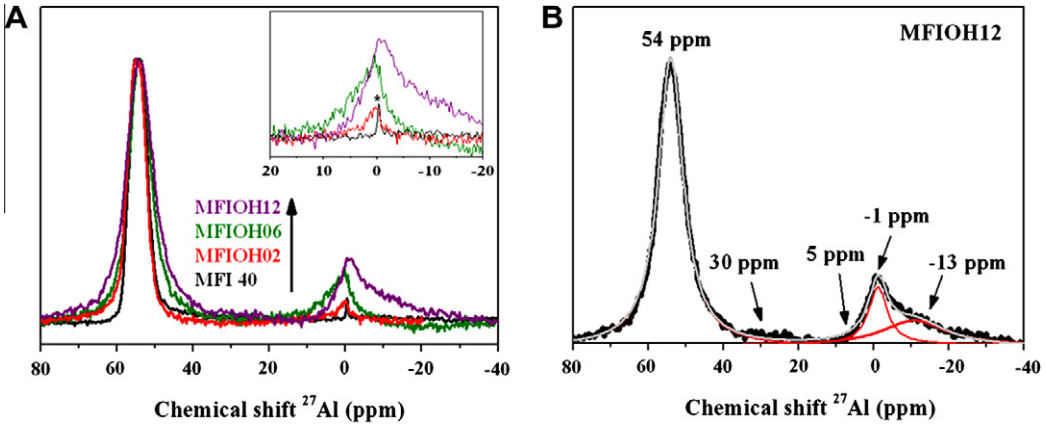

Fig. 4. (A) ^{27}Al NMR spectra of parent and desilicated zeolites and (B) deconvolution of MFIOH12 spectra. The relative areas of the resonances peaks are given in Table 2.

Table 2
Relative population distribution of aluminum species in parent MFI40 and desilicated zeolites. Each family was integrated separately after deconvolution of ^{27}Al NMR spectra.

Coordination	δ (ppm)[a]	Species of ^{27}Al distribution (%)					
		MFI40	MFIOH02	MFIOH04	MFIOH06	MFIOH08	MFIOH12
AlO_4	54[b]	98.8 (5.4)[c]	96.3 (5.6)	83.6 (6.1)	76.5 (6.6)	65.8 (6.1)	71.7 (8.0)
AlO_5	30	0	0	0	0	0	1.3
AlO_6-I	5	1.2	3.7	8.8	9.7	4.4	0
AlO_6-II	−1	0	0	7.6	13.9	11.1	10.8
AlO_6-III	−13	0	0	0	0	18.6	16.2

[a] Average chemical shift.
[b] This signal is assigned to the zeolite framework aluminum.
[c] The width of the peak at middle height (in ppm), showing the broadening of this signal according to desilication degree.

influence of microporosity and confinement effect on physisorbed ammonia, Py-FT-IR was also used as complementary characterization.

The typical TPD curves from the acid zeolites with different aluminum contents are shown in Fig. 5A and B. The curves present two desorption peaks, termed l- and h-peaks, that is, low and high temperatures, respectively. According to several references [21], ammonia molecules showing the h-peak are related to the aluminum atoms in the zeolite framework for the H-form zeolite samples with high crystallinity. On the other hand, the l-peak is

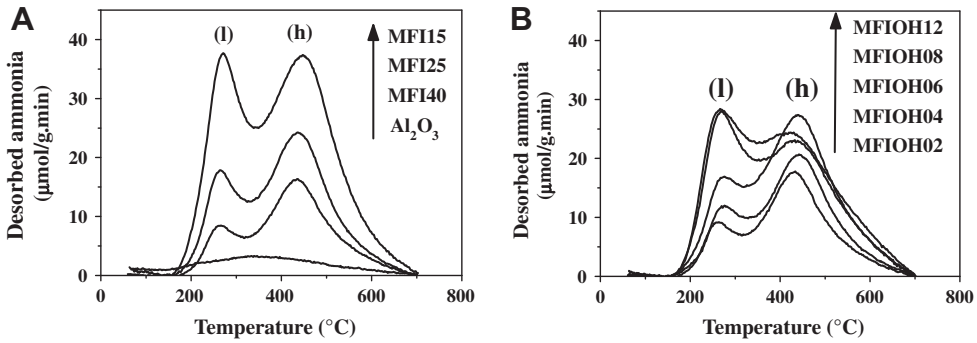

Fig. 5. Temperature-programmed desorption profiles of adsorbed ammonia (A) parent catalysts and reference alumina and (B) desilicated MFI40 zeolite.

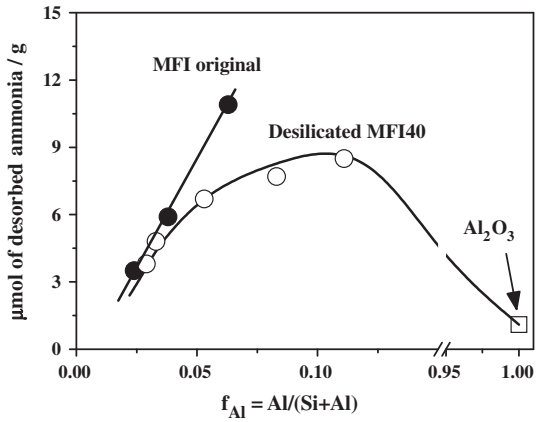

Fig. 6. Plot of the acid amount determined from the whole desorbed peak area of ammonia against aluminum fraction in the solid (framework and non-framework aluminum species are included in the calculation). Filled points correspond to parent zeolites containing only tetrahedrally coordinated framework aluminum, and the empty points to MFI40 zeolite desilicated in different volumes of NaOH solution.

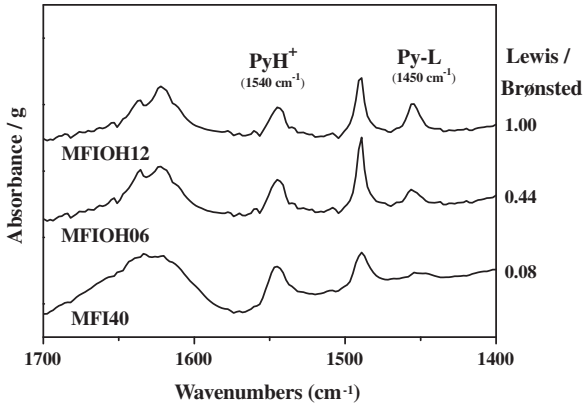

Fig. 7. IR spectra of pyridine adsorbed on the zeolites after desorbing weakly bond species at 150 °C. The relative intensities between pyridine chemisorbed on Lewis and Brønsted sites is indicated.

found even for the sodium form zeolite, and its presence might correspond to ammonia molecules more strongly physisorbed in the micropores [22]. The interpretation of TPD data might be somewhat complex and not straightforward. For instance, some authors [21] suggest also that the l-peak is associated either with the higher concentration of extra-framework aluminum species or with the silanol groups on the external surface of the zeolite crystals. In the current study, no relation between l- and h-peak and acid or textural characteristics could be drawn for these samples; however, the integration of the entire desorbed curves allowed us to gather information about the different nature of the acid sites, such as the parent samples in which the TPD peak area increased with increasing aluminum fraction (closed symbols in Fig. 6). Evidently, this is a consequence of the increasing presence of Brønsted acid sites in the parent samples. For the desilicated MFI40 samples, the amount of chemisorbed ammonia goes through a maximum, as desilication is more severe due to an increase in the Lewis acid species, especially alumina outside the network. The reference alumina, which presented a very low and broad temperature desorption peak, presents a negligible amount of chemisorbed ammonia reinforcing the weak characteristic of Lewis sites for this sample.

More qualitative determination of the Brønsted and Lewis acid sites was carried out using the IR bands at 1540 cm^{-1} (PyH^+) and 1450 cm^{-1} (PyL) after adsorption of pyridine (Fig. 7) [3,23]. These IR bands are the characteristic ones to probe pyridine that interact with the acid sites. After the alkaline treatment, the total Brønsted acid sites concentration decreased due to framework desilication. Notably, the most significant changes in Lewis/Brønsted ratio occurred more seriously for the MFIOH12 zeolite, which exhibited relative intensity of sites of 1.0. For the parent MFI40 zeolite, nearly only Brønsted sites are present. This result strongly supports that the parent zeolites present remarkably more Brønsted acid sites, that is, stronger acidic hydroxyl groups, in comparison with desilicated zeolites. However, in a realistic analysis of industrial applications of these materials, the slow diffusion in purely microporous zeolite crystals can lead to low catalytic selectivity and durability due to diffusion problems and to coke formation.

By combining the results from Figs. 6 and 7, we can conclude that the desilicated zeolites possess somewhat weaker acid strength than the parent zeolites with the same aluminum fraction, but still a well-designed pore structure that can allow for a rapid diffusion and, consequently, improve the reaction kinetics as measured by catalytic glycerol dehydration.

3.3. Glycerol dehydration: activity, selectivity to acrolein, and catalyst deactivation

The main reaction product found during glycerol dehydration was acrolein and minor products were acetol, acetaldehyde, allyl alcohol, propanal, and heavy coked compounds, which were not identified but were quantified through carbon balance (C_{out}/C_{in} molar ratio in Fig. 8). Missing carbon could also be due to some minor unknown components detected in chromatograms. We did not detect the formation of acetic acid nor acrylic acid, products resulting from oxydehydration of glycerol. Because of the relatively low temperatures needed for dehydration, the reaction of glycerol

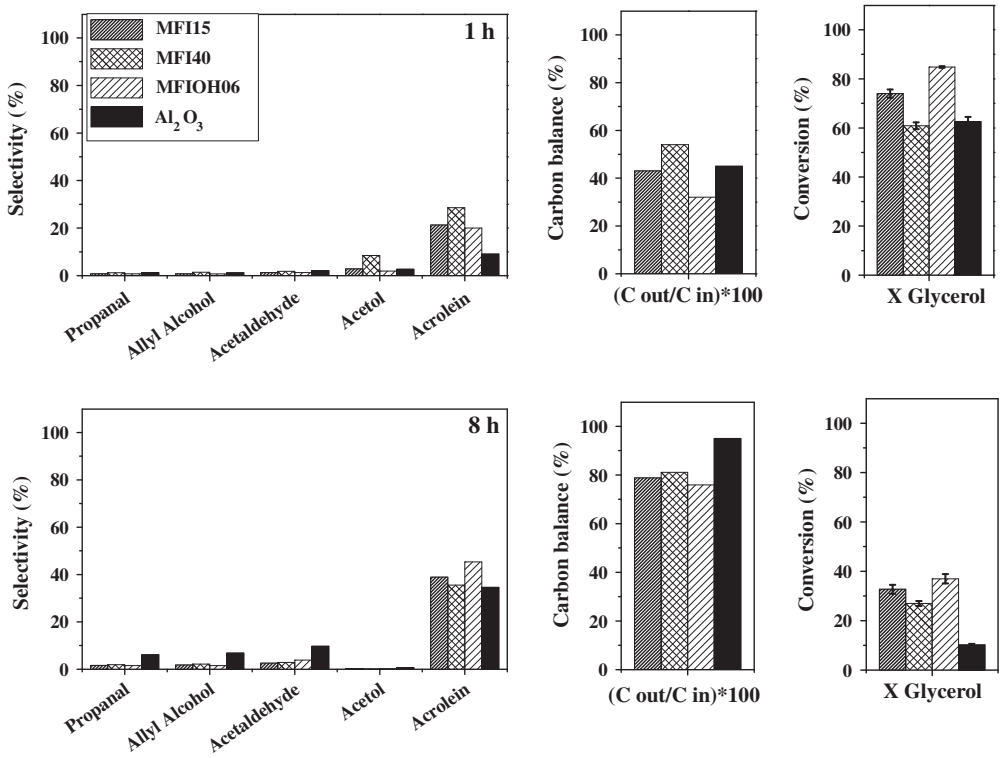

Fig. 8. Effect of reaction time on catalytic behavior (glycerol conversion, products selectivity, and carbon balance) of MFI15, MFI40, MFIOH06 zeolites and of the commercial alumina. In some cases, the error bars are smaller than the size of the points.

reforming as a possible parallel reaction was completely suppressed at the temperature of 300 °C. In Fig. 8, error bars based on standard deviation of three GC injections of the same sample were added in order to highlight that the differences between samples are significantly consistent.

The very low carbon balance during catalytic reaction and the black appearance of used catalysts suggested the significant formation of coke, influencing negatively the selectivity to acrolein. However, if only the volatile products flowing out of the reactor were considered, acrolein itself would contribute to the higher yield. The deactivation was also confirmed and quantified by experiments carried out under isothermal conditions at 300 °C for 8 h.

Fig. 9 shows a reasonable scheme to explain glycerol dehydration on Brønsted and Lewis acid sites to produce acrolein and major co-products revealed in Fig. 8 [1]. In the Brønsted sites, there are two events of dehydration and these events are in series. The glycerol secondary hydroxyl group is readily protonated in step (1). Subsequently, there is the formation of an intermediate, 1,3-dihydroxipropene (step 2, the first dehydration), and after that, a keto-enol rearrangement leads to 3-hydroxypropanal (3). In step (4), the catalyst is regenerated. After the formation of 3-hydroxypropanal (3), the second dehydration occurs through the protonation of the remaining hydroxyl group to produce acrolein (5). In the step 6, the catalyst is regenerated. The parallel reaction of glycerol dehydration (1) on Lewis acid sites occurs via interaction of a terminal hydroxyl group and there is the transference of the secondary proton to surface oxygen atoms. Then, the formation of 2,3-dihydroxypropene (2) occurs and the keto–enol rearrangement allows the production of acetol (3) [1]. The origin of the remaining and less abundant by-products is not so clear. One obvious explanation is that all of these compounds can be derived from the chemical modification or bond scissions of other products.

The dehydration of glycerol was also carried out on the parent and desilicated zeolites for different times on stream, and the variations of the glycerol conversion are shown in Fig. 10A. In order not to consider the influence of the deactivation in the interpretation of the catalysts activity, the results shown in Fig. 10C have been achieved by extrapolating the curves in Fig. 10A to reaction time = 0. In an additional effort to explore the effect of porosity and to exclude the influence of deactivation and coke deposition, we also conducted ethanol dehydration reaction, which is a known and non-deactivating reaction (Fig. 10B) [24].

The curves of Fig. 10C and D clearly show that the catalytic activity of desilicated samples in both catalytic reactions undergoes a maximum – in a similar manner to the behavior noticed in the desorption of ammonia of the same catalysts. There is, however, another factor that contributes to the catalytic activity besides the varying amount of acid sites, which is probably caused by the increase in mesopores volume in the desilicated zeolites crystals. The curves in Fig. 10C and D were separated in two regions: region 1, which corresponds to desilicated zeolites that have higher catalytic activity when compared to parent zeolites with the same amount of aluminum atoms and region 2, which corresponds to severely desilicated and crystalline damaged zeolites with lower activity. Notice the increase in MFIOH04 conversion in relation to MFI40. There is a maximum in the conversion in MFIOH06 zeolite and then a subsequent decrease with increasing desilication in MFIOH12, which can be explained by the degradation of the zeolite structure with the strong basic treatment. A similar behavior is also detected for the dehydration of ethanol, reinforcing the observation that the combination of appropriate surface acidity and well-designed pore structure allows for a rapid diffusion and consequently improves the reactant conversion.

Fig. 10C shows that, as expected, the increasing amount of aluminum of the parent catalysts increases glycerol conversion as a consequence of the presence of more acid sites. In order to verify the intrinsic activity of the acid sites of each sample, the conversion rate of glycerol per aluminum mol present in the catalyst was estimated (TOF – turnover frequency measurements in Table 3

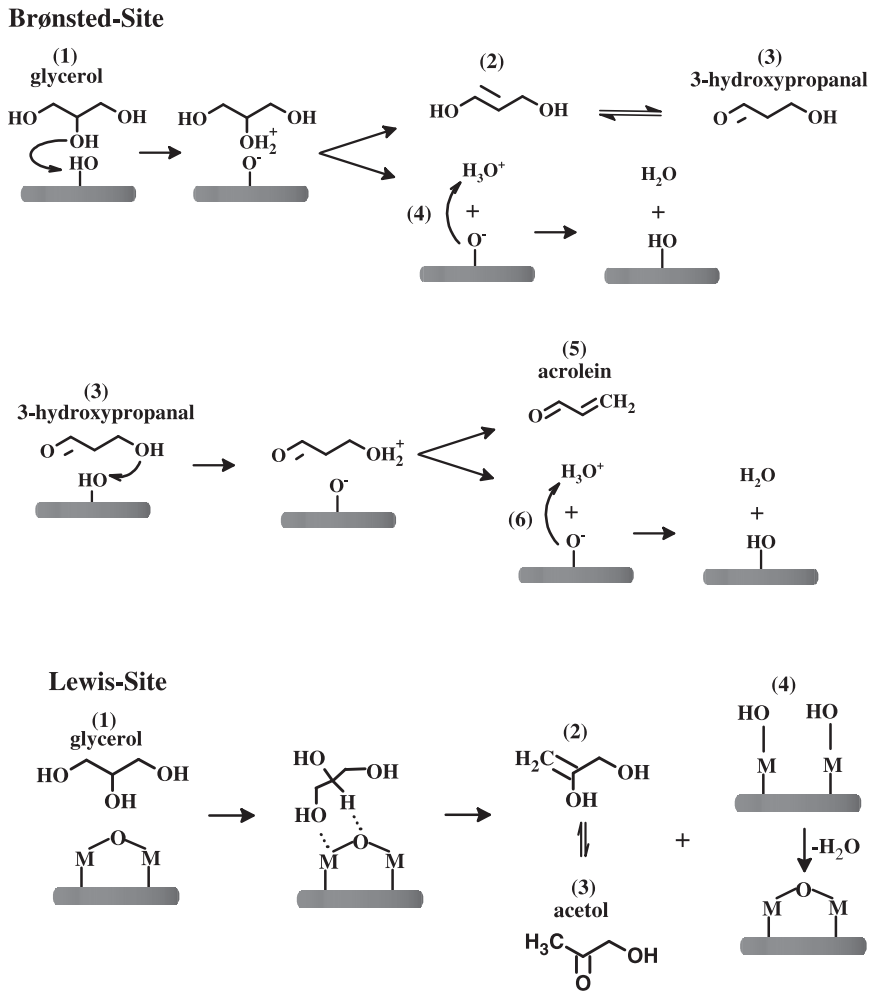

Fig. 9. Probable and simplified reaction steps during glycerol dehydration on Brønsted and Lewis acid sites, which corresponds to a series–parallel reaction network [1].

and in Fig. 1 of supplementary material). A regular increase in TOF with decreasing aluminum contents in the zeolites was found. The increasing TOF number as aluminum contents decreases is a known property for zeolites and is related to a lower negative charge density in the zeolite framework, which contributes to stronger Brønsted acid sites. Comparing the same amount of aluminum, the micro-mesoporous zeolites are more active based on the TOF numbers. The figure included in Supplementary material shows that the higher TOF values for the same Si/Al ratio are attributed to the creation of mesoporosity in the zeolite crystals having more accessible acid sites that provide the benefit of enhanced mass transfer and higher catalytic activity. The differences between desilicated and parent zeolites are more evident for less desilicated zeolites, because the zeolitic structure is more preserved and the Brønsted acid sites are more abundant. For the severely alkaline-treated samples, that is, MFIOH08 and MFIOH12, the TOF values are lower than the parent zeolites due to the existence of less acidic Lewis sites and occasionally blockage of micropores due to the presence of extra-framework aluminum species.

The change in the relative abundance of Lewis and Brønsted acid sites is one of the probable reasons for the different selectivity of acrolein and acetol, because, as mentioned and discussed in Fig. 9, dehydration may go through different catalytic sorption processes. Table 3 indicates that for desilicated zeolites, the selectivity to acrolein decreases while to acetol increases, that is, the acetol/acrolein molar ratio increases regularly from 0.01 to 0.23. However, the increase in acetol formation is not proportional to the relative quantity of Lewis/Brønsted sites. For example, despite the fact that the sample MFIOH12 exhibited relative intensity of Lewis/Brønsted sites of 1.0 as revealed by pyridine chemisorption, the selectivity to acetol is five times lower compared to acrolein. The interpretation of this behavior and the use of the reference alumina as catalyst reinforce the weak characteristic of Lewis sites for glycerol conversion to acetol. Predominantly for the parent zeolites, the acetol/acrolein molar ratio was rather different from desilicated zeolites (in the range between 0.13 and 0.30). In this case, we attribute that to the presence of very low quantity of distinct nanometric extra-framework aluminum species in the parent zeolites, which are easily leached in the presence of a few milliliters of sodium hydroxide solution used in the preparation of sample MFIOH02. The insert in Fig. 4A indicates a narrow peak around 0 ppm for the parent zeolite and a broad one for the MFIOH02, although both samples have nearly the same framework Si/Al molar ratio (Table 1).

The comparison depicted in Fig. 8, for two different reaction times of several catalysts (1 and 8 h), allows the confirmation that the decrease in selectivity with time is due to coke deposits. Fig. 8 also reveals that during the dehydration reaction, the selectivity to acrolein is increased. The reason is that this product is formed on strong acid sites (Brønsted), while others, such as acetol and acetaldehyde are formed on sites of weak acidity (Lewis) that rapidly

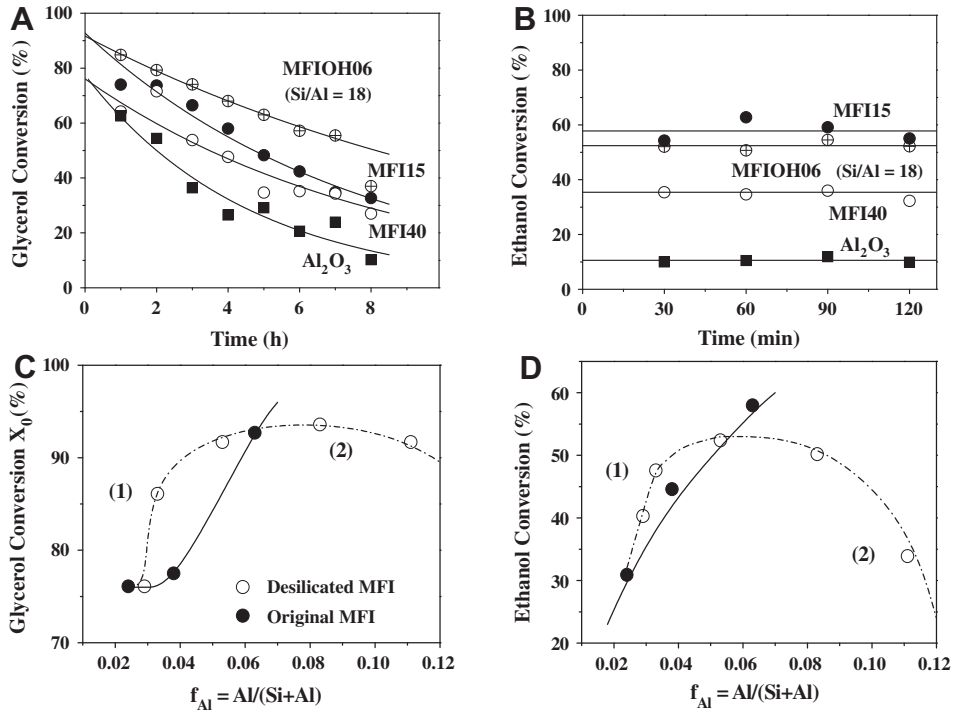

Fig. 10. (A) Glycerol conversion, (B) ethanol conversion, (C) glycerol conversion (X_0) of original and desilicated zeolite, and (D) ethanol conversion of original and desilicated zeolite.

Table 3
Main results obtained from dehydration of glycerol using parent and desilicated zeolites: TOF, selectivity to acrolein and acetol and deactivation detected after 8 h of reaction.

Treatment	Sample	Si/Al	TOF_0 [a] (1/s)	S_0 acrolein[b] (%)	S_0 acetol[b] (%)	Acetol/acrolein molar ratio	Deactivation 8 h (%)[c]
Parent	MFI15	15	13.2	21.3	2.8	0.13	64.9
	MFI25	25	19.3	18.4	3.3	0.18	68.5
	MFI40	40	29.3	19.9	2.1	0.30	61.9
Desilicated MFI40	MFIOH02	34	33.0	20.1	0.2	0.01	61.8
	MFIOH04	29	24.5	20.4	1.0	0.02	58.5
	MFIOH06	18	17.9	20.0	1.9	0.10	44.9
	MFIOH08	11	11.3	26.2	2.4	0.09	61.7
	MFIOH12	08	8.6	15.1	3.4	0.23	60.1
Reference	Al_2O_3	...	...	9.1	2.7	0.30	82.7

[a] TOF_0: zero time extrapolated turn over frequency, based on glycerol conversion at time zero.
[b] Selectivity to acrolein and acetol at time zero.
[c] Deactivation estimated based on time zero and final glycerol conversion after 8 h of reaction.

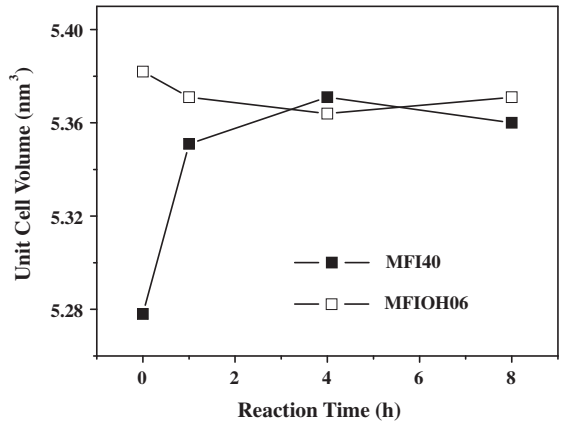

Fig. 11. Progression of unit cell volume expansion of used MFI zeolite due to coke deposition in the micropores, as measured by X-ray diffraction after different reaction times.

Table 4
Comparison of structural parameters for the MFI zeolites before and after glycerol dehydration.

Parameters	Fresh catalysts (0 h)			Used catalysts (8 h)		
	MFI40	MFI25	MFIOH06	MFI40	MFI25	MFIOH06
β (°)	90.176	90.176	90.050	90.307	90.129	90.202
a (nm)	1.984	1.984	2.005	1.997	2.003	2.009
b (nm)	1.992	1.992	2.005	2.005	2.001	1.992
c (nm)	1.336	1.335	1.339	1.339	1.342	1.342
V (nm^3)	5.278	5.278	5.382	5.360	5.377	5.371

deactivate by coke deposition. The high deactivation of alumina of 82.7% indicated in Table 3 explains this result.

3.4. A microscopic picture of the zeolites deactivation in glycerol dehydration

A comparison of the catalysts reveals that, besides the acidity, the decrease in glycerol conversion is also influenced by the struc-

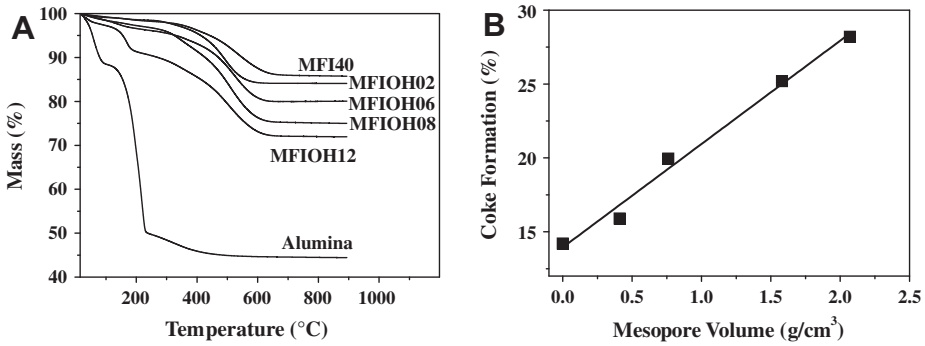

Fig. 12. (A) Thermogravimetric curves of used catalysts after 8 h in dehydration of glycerol; (B) correlation between mesopores volume and relative mass percentage measured in the temperature range of 150–700 °C.

ture and the textural properties of the solids. The deactivation, which was estimated from initial and final glycerol conversion after 8 h of reaction, showed a minimum value centered on MFIOH06 zeolite which presents pores and active sites more accessible to glycerol molecules, despite the more weakly acidic sites that are exposed.

A microscopic picture of the deactivation by coke deposition into the hierarchical channel system created between micro- and mesopores can be drawn as follow. We supported our discussion using a combination of measurements of unit cell parameters of MFI zeolites presented in Fig. 11 and Table 4, and thermogravimetric curves presented in Fig. 12. The structural parameters (Table 4), as measured by X-ray diffraction after different reaction times, show that the structure of MFI40 sample expands for increasing reaction times probably due to deposition of bulky molecules in the micropores. Access of bulky molecules is to some extent limited to zeolite pores so that only molecules having effective diameters small enough can enter without restraint. Consequently, this result supports that reactant molecules enter the pores and coke formation initiates inside zeolite cavities. In fact, micropore volume diminishes deeply, from 0.29 to 0.00 mL/g (Table 1), as measured for MFI25 sample after 8 h in glycerol dehydration. The X-ray diffraction studies suggest a rather continuous flexibility of the zeolite framework during coke formation [25]. The unit cell volume in MFI40 increased from 5.278 nm^3 to 5.371 nm^3 after 8 h of reaction, reaching saturation at 5.377 nm^3. The three directions of the unit cell expanded equally for all the studied zeolites (Table 4). Such changes strongly suggest that coke in the zeolite resides not only in the channel along the "*b*" axis (the straight channel) but also in the channel along the "*a*" axis (the sinusoidal channel) [26]. The calculated parameters for fresh MFIOH06 zeolite, as revealed by the lower β (°) value, show less severe distortion of silicon and aluminum atoms in the channels and higher surface defects of this zeolite when compared to the parent ones. Curiously, this zeolite did not expand for different reaction times possibly due to the less efficient blocking of MFI micropores in accordance with the lower deactivation of 44.9% registered in glycerol dehydration and the less intense decay of pore volume revealed by nitrogen adsorption of the used catalyst. However, a very contrasting and intriguing result was observed for this sample: despite the lower deactivation, a higher amount of carbonaceous deposits was detected in comparison with parent zeolites. From the thermogravimetric results after catalytic glycerol dehydration, it was possible to establish a linear dependence between the mesopore volume and the amount of carbonaceous compounds deposited on the catalysts (Fig. 12B). As shown in Fig. 12A, the parent MFI40 zeolite presents a mass percentage of approximately 15 %, while the most desilicated sample, MFIOH12, loses 30% of the initial mass. The reference alumina shows the higher amount of carbon deposit.

The scheme presented Fig. 13 provides a simplified microscopic picture of the deactivation by deposition of coke on the different catalysts: (1) in the case of purely microporous zeolites, the coke is essentially deposited within straight and sinusoidal micropores

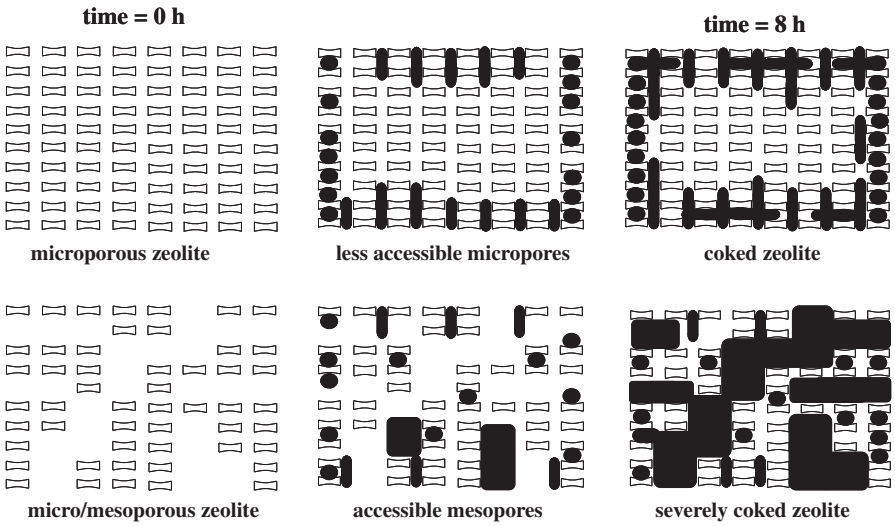

Fig. 13. Schematic representation of the domains of coke deposition and location in the pores during glycerol dehydration on (a) purely microporous zeolites and (b) micro- and mesoporous zeolites.

and its effect on catalytic performance is more pronounced even for low coke content, caused by pore blockage obstructing the access of glycerol to narrow channels located deep in the crystals; (2) in the case of micro- and mesoporous zeolites, the coke is not deposited in narrow micropores as confirmed from the insignificant changes in crystallographic parameters of the zeolite, but are preferentially located in the intracrystalline pockets created by means of desilication. This behavior originates from the change of location of most of the active sites as well as from the easier retention of coke molecules in non-confined environments, typical of purely microporous zeolites.

The catalysts used in this study do not present the best selectivity to acrolein when compared to other catalysts, whose selectivity usually goes beyond 80%. Obviously, this depends strongly on the reactions conditions. For example, in this study, a mixture of 10 wt.% of glycerol in water was used to efficiently feed glycerol into the reactor; however, water can strongly adsorb on the surface acid sites of the solid acid catalysts and disturb the adsorption of accessible reactants. Further on, the most important contribution of this study was to compare the catalysts and to reveal that, besides the acidity, the conversion of glycerol and catalyst stability are indeed influenced by the structure and the textural properties of the solids.

4. Conclusions

In this study, the effect of desilication in the conversion of glycerol, the distribution of the products and also the control of diffusion constraints, and deactivation by different location of coke formation in the pores of mono- and bimodal zeolites was shown. For the obtained zeolites, the catalytic activity in glycerol dehydration went through a maximum as a function of desilication procedure. This behavior can be explained by the combination of antagonist properties: decrease in strength of surface acidity and increase in mesoporosity and accessibility of glycerol to active sites. The characterization techniques TPD of ammonia and IR of chemisorbed pyridine showed the presence of Brønsted acid sites in the parent samples and increased amount of Lewis acid species in severe desilicated zeolites. In the case of micro-mesoporous zeolites, coke is preferentially deposited in the intracrystalline pockets created by means of desilication resulting in more stable catalysts. This study highlights that both porosity and acidity must be considered in the evaluation of the overall activity of porous catalysts prepared by similar procedures.

Acknowledgment

The authors acknowledge financial support from the FAPESP, CNPq and CAPES/Brazil.

Appendix A. Supplementary material

Supplementary data associated with this article can be found, in the online version, at http://dx.doi.org/10.1016/j.jcat.2013.01.003.

References

[1] B. Katryniok, S. Paul, V.B. Baca, P. Rey, F. Dumeignil, Green Chem. 12 (2010) 2079–2098.
[2] H. Serafim, I.M. Fonseca, A.M. Ramos, J. Vital, J.E. Castanheiro, Chem. Eng. J. 178 (2011) 291–296.
[3] E. Yoda, A. Ootawa, Appl. Catal. A: Gen. 360 (2009) 66–70.
[4] J. Deleplanque, J.L. Dubois, J.F. Devaux, W. Ueda, Catal. Today 157 (2010) 351–358.
[5] C.J. Jia, Y. Liu, W. Schimidt, A.H. Lu, F. Schuth, J. Catal. 269 (2010) 71–79.
[6] A. Witsuthammakul, T. Sooknoi, Appl. Catal. A 413–414 (2012) 109–116.
[7] W. Suprun, M. Lutecki, R. Glaser, H. Papp, J. Mol. Catal. A: Chem. 342–343 (2011) 91–100.
[8] A. Ulgen, W.F. Hoelderich, Appl. Catal. A: Gen. 400 (2011) 34–38.
[9] Y.T. Kim, K.D. Jung, E.D. Park, Appl. Catal. A: Gen. 393 (2011) 275–287.
[10] C.J. A Mota, C.X.S. Silva, V.L.C. Gonçalves, Quim. Nova 32 (2009) 639–648.
[11] A. Corma, Chem. Rev. 95 (1995) 559–614.
[12] R.A. Sheldon, R.S. Dowing, Appl. Catal. A 189 (1999) 163–183.
[13] K. Egeblad, M. Kustova, S.K. Kiltgaard, K. Zhu, Micropor. Mesopor. Mater. 101 (2007) 214–223.
[14] R. Chal, C. Gérardin, M. Bulut, S. Donk, ChemCatChem 3 (2011) 67–81.
[15] D. Verboekend, J.P. Ramírez, Chem. A Eur. J. 17 (2011) 1137–1147.
[16] J.P. Lourenço, M.I. Macedo, A. Fernandes, Catal. Commun. 19 (2012) 105–109.
[17] D. Verboekend, J.P. Ramíres, Chem. Eur. J. 17 (2011) 1137–1147.
[18] R.M. Mihályi, M. Kollár, P. Király, Z. Karoly, V. Mavrodinova, Appl. Catal. A: Gen. 417–418 (2012) 76–86.
[19] J. Xia, D. Mao, W. Tao, Q. Chen, Y. Zhang, Y. Tang, Micropor. Mesopor. Mater. 91 (2006) 33–39.
[20] A. Gola, B. Rebours, E. Milazzo, J. Lynch, E. Benazzi, S. Lacombe, L. Delevoye, C. Fernandez, Micropor. Mesopor. Mater. 40 (2000) 73–83.
[21] A.W. Chester, E.G. Derouane (Eds.), Zeolite Characterization and Catalysis: A Tutorial, Springer, 2009, p. 358.
[22] N. Katada, M. Niwa, Catal. Surv. Asia 8 (2004) 161–170.
[23] F. Jin, Y. Li, Catal. Today 145 (2009) 101–107.
[24] L. Martins, D. Cardoso, P. Hammer, T. Garetto, S.H. Pulcinelli, C.V. Santilli, Appl. Catal. A: Gen. 398 (2011) 59–65.
[25] L. Martins, R.T. Boldo, D. Cardoso, Micropor. Mesopor. Mater. 98 (2007) 166–173.
[26] T. Ohgushi, T. Niwa, H. Araki, S. Ichino, Micropor. Mater. 8 (1997) 231–239.